Equivalent: Jurnal Ilmiah Sosial Teknik
Volume 8, Issue 4, 1474-1488
e_ISSN: 2775-0833
https://jurnalequivalent.id/index.php/jequi/index
DOI: doi.org/10.59261/jequi.v8i4.421

Failure Analysis of High Pressure Shaft Pump Sea Water Reverse Osmosis in the Labuhan Angin Generation Business Unit

Wandi Pagar Asi Napitupulu*
Institut Teknologi Sepuluh Nopember, Indonesia

Fahmi Mubarok
Institut Teknologi Sepuluh Nopember, Indonesia

***Corresponding author:**
Wandi Pagar Asi Napitupulu, Institut Teknologi Sepuluh Nopember Indonesia. ✉6007241068@student.its.ac.id

Article Info:
Article history:
Received: July 21, 2026
Revised: September 01, 2026
Accepted: September 04, 2026
Available Online: September 07, 2026

Keywords:
Failure Analysis; Power Plant; Pump; Shaft; Water Treatment.

Abstract

Background: UBP Labuhan Angin relies on the high-pressure (HP) pump in the seawater reverse osmosis system to maintain the availability of boiler feedwater and the readiness of the power plant. Repeated shaft failures may disrupt the water-treatment process and compromise the reliability of electricity generation.
Objective: This study analyzed the factors contributing to the failure of the HP pump shaft at UBP Labuhan Angin.
Methods: The study employed chemical composition testing, macrographic and micrographic examinations, scanning electron microscopy, and Vickers hardness testing.
Results: The findings showed that the hardness values of Materials A and B were nonuniform and lower than the reference value for AISI 440A. Material A had a lower carbon content, whereas Material B had a lower chromium content than the specified ranges. Fractographic and microstructural observations indicated brittle fracture, crack initiation in the central area, chromium carbide precipitation, and nonuniform effects of heat treatment.
Conclusion: The shaft failure was associated with deviations in chemical composition, insufficient and nonuniform hardness, brittle fracture characteristics, and an inappropriate heat-treatment process, which reduced the material's resistance to cyclic operational loads.

To cite this article: Napitupulu, W. P. A., & Mubarok, F. (2026). Failure Analysis of High Pressure Shaft Pump Sea Water Reverse Osmosis in the Labuhan Angin Generation Business Unit. *Equivalent: Jurnal Ilmiah Sosial Teknik*, 8(4), 1474-1488. https://doi.org/10.59261/jequi.v8i4.421

INTRODUCTION

The need for electrical energy plays an important role in supporting a country's development. In Indonesia, the demand for electrical energy increases every year (Amin et al., 2023). To meet this demand for electrical energy, a high level of power plant readiness is required (Wulandari & Alifah, 2026).

Maintaining power plant readiness requires effective water treatment within the power generation process (Inyang & Olughu, 2025), as water quality affects the quality of the water that will be processed into steam. Poor water quality can cause problems in other critical components, such as boilers and turbines.

In the water treatment process of a power generation system, the high-pressure (HP) pump functions to transfer water and increase its pressure before it enters the sea water reverse osmosis (SWRO) system (Joniarta et al., 2024). The high pressure required in the SWRO process is necessary to overcome the natural osmotic pressure of seawater, which has a high salt concentration (Rifai et al., 2024). Conversely, if the pressure supplied to the SWRO system is too low, it will affect the quality of the water produced, including its conductivity and other chemical parameters. Disruptions in the performance of HP pumps will not only affect the quality of the product water but also the volume of water produced (Dwiyoga, 2024).

On this basis, HP pumps play a vital role in the water treatment process at the plant (Wahyudin et al., 2024). The reliability and availability of the HP pump play an important role in maintaining plant readiness and ensuring a continuous electricity supply.

Figure 1. HP Pump SWRO UBP Labuhan Angin
(Source: Private archive, 2025)

As is also the case at UBP Labuhan Angin, the availability of HP pumps as vital equipment in the water treatment process is an important aspect that must be monitored. Operational records at UBP Labuhan Angin documented several incidents of HP pump performance failures, indicating a recurring technical problem that required further investigation.

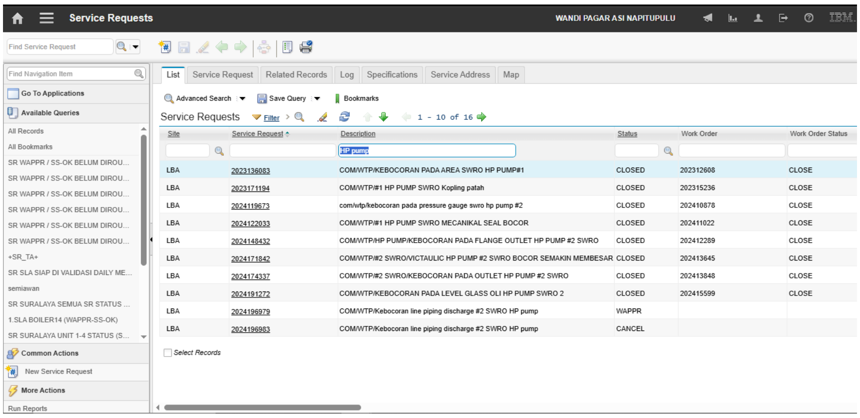

Service Requests

Site	Service Request	Description	Status	Work Order	Work Order Status
LBA	2023136083	COM/WTP/KEBOCORAN PADA AREA SWRO HP PUMP#1	CLOSED	202312608	CLOSE
LBA	2023171194	COM/WTP/#1 HP PUMP SWRO Kopling patah	CLOSED	202315236	CLOSE
LBA	2024119673	com/wtp/kebocoran pada pressure gauge swro hp pump #2	CLOSED	202410878	CLOSE
LBA	2024122033	COM/WTP/#1 HP PUMP SWRO MECANIKAL SEAL BOCOR	CLOSED	202411022	CLOSE
LBA	2024148432	COM/WTP/HP PUMP/KEBOCORAN PADA FLANGE OUTLET HP PUMP #2 SWRO	CLOSED	202412289	CLOSE
LBA	2024171842	COM/WTP/#2 SWRO/VICTAULIC HP PUMP #2 SWRO BOCOR SEMAKIN MEMBESAR	CLOSED	202413645	CLOSE
LBA	2024174337	COM/WTP/#2 SWRO/KEBOCORAN PADA OUTLET HP PUMP #2 SWRO	CLOSED	202413848	CLOSE
LBA	2024191272	COM/WTP/KEBOCORAN PADA LEVEL GLASS OLI HP PUMP SWRO 2	CLOSED	202415599	CLOSE
LBA	2024196979	COM/WTP/Kebocoran line piping discharge #2 SWRO HP pump	WAPPR		
LBA	2024196983	COM/WTP/Kebocoran line piping discharge #2 SWRO HP pump	CANCEL		

Figure 2. HP Outage Notes Pump SWRO UBP Labuhan Angin (Data obtained from individuals, 2025)

In this study, the HP pump performance failure was caused by a fractured shaft on the motor side that occurred on July 8, 2025. Based on operational records, similar incidents had also occurred four times previously, although not all of them were recorded in the system, namely, on June 4, 2025, June 11, 2025, June 15, 2025, and June 28, 2025. The series of repeated failures indicates fundamental problems with the shaft components that need to be further analyzed to identify the root cause of the failure and prevent similar damage in the future.

Figure 3. Shaft Fracture on HP Pump SWRO Date June 11, 2025
(Source: Private archive, 2025)

Before each shaft failure, the operational data showed similar characteristics: the coupling housing temperature exceeded 90 °C, and the motor current exceeded 295 A. Subsequently, the motor current suddenly decreased to below 60 A, accompanied by a low-pressure alarm and a substantial reduction in discharge flow. These conditions indicated an operating failure of the HP pump, which was subsequently confirmed by the discovery of a fractured shaft at the coupling.

Repeated shaft failures in the SWRO HP pump have the potential to disrupt the continuity of the power supply. Therefore, an analysis is needed to identify the factors causing the failures as a mitigation effort to prevent similar incidents from occurring in the future. This study aims to analyze and identify the cause of shaft failure in the SWRO HP pump at UBP Labuhan Angin. The scope of the research is limited to the HP pump shaft at UBP Labuhan Angin and includes analysis of the test material and available technical data using chemical composition analysis, fractography, scanning electron microscopy (SEM), and mechanical property testing.

This research provides both scientific and practical benefits. Academically, this research contributes to expanding the understanding of material failure analysis in the field of power generation, particularly with regard to the failure mechanisms of rotating components. Practically, the results of this study can be used to identify the cause of failure of the HP SWRO pump shaft and provide a basis for improvement recommendations to enhance reliability and optimize the performance of the UBP Labuhan Angin plant in the future.

METHOD

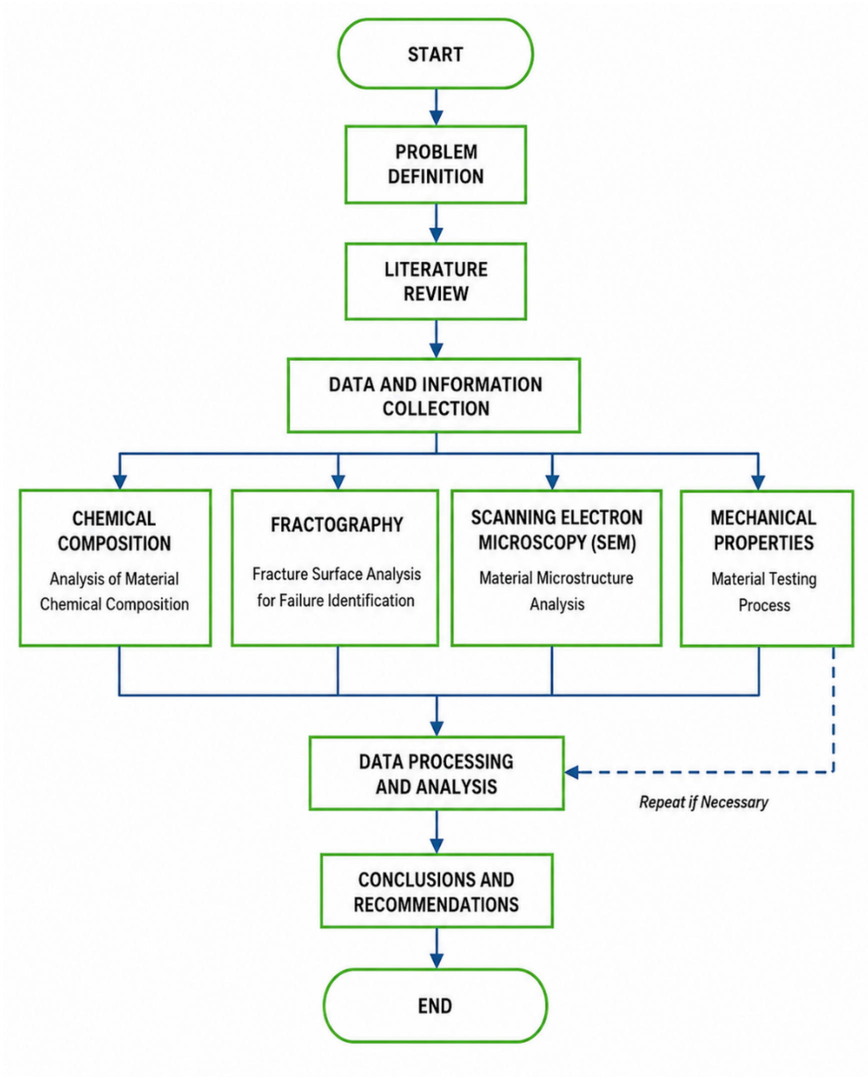

Figure 4. Research Flow Diagram

Determination of boundaries and formulation of the problem is an important first step in determining a clear scope and focus of research. Through root cause failure analysis (RCFA), it can help in the formulation of problems in a structured and logical manner.

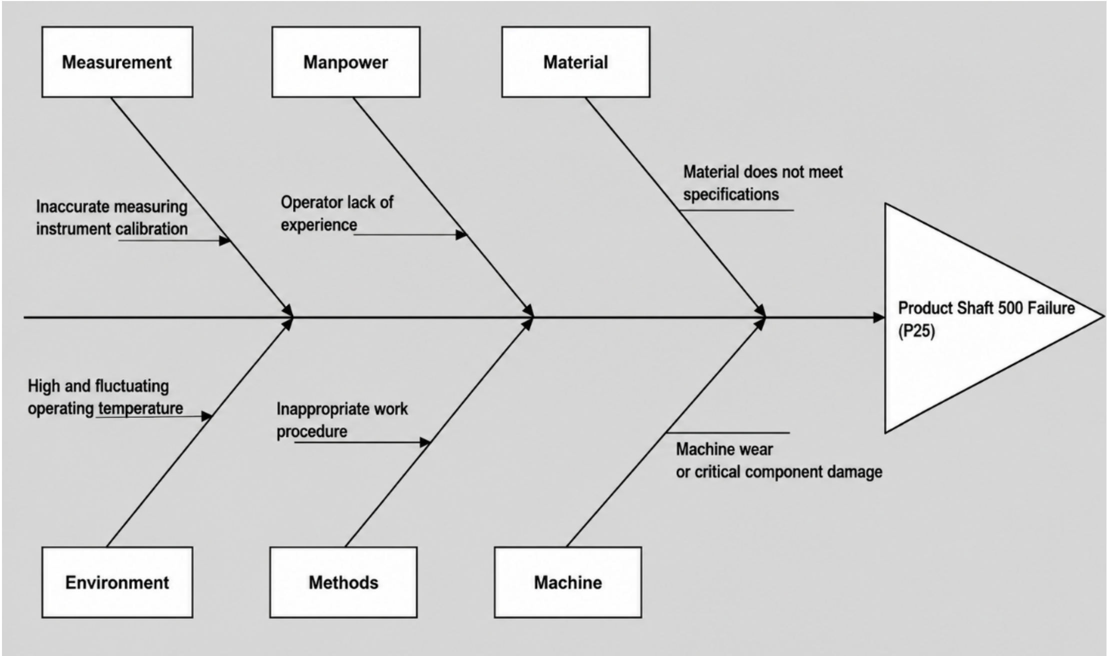

Figure 5. RCFA Problem Formulation of HP Pump SWRO Shaft Failure Analysis

The literature review provided a theoretical foundation for identifying unresolved research gaps. Comparing the findings of the present study with those of previous studies also helped prevent unnecessary duplication and strengthened the originality of the research.

The data collection strategy was designed to provide a comprehensive perspective for addressing the research objectives. In this study, data were collected using several methods, namely:

1) Macroscopic examination: This method was used to identify and measure initial fracture features, such as beach marks and shear-lip patterns.
2) Microscopic examination: This method was used to examine the microstructure around the fracture, including grain size and indications of plastic deformation or cleavage.
3) Scanning electron microscopy (SEM): SEM was used to obtain high-resolution images of the fracture surface from the area of crack initiation to the propagation region, enabling the identification of fatigue features and the presence of dimples.
4) Destructive testing: This method was used to obtain mechanical property data for the material.

The research was conducted in a materials laboratory using the tools and materials required for the study, as follows:

1) Failure specimens
2) HP pump design manual for UBP Labuhan Angin
3) HP pump trending and operational data from UBP Labuhan Angin
4) Camera
5) Optical microscope
6) Scanning electron microscope (SEM)
7) Vickers hardness tester

Using the data collection strategy and the available tools and materials, this study targeted detailed and measurable outputs in the following forms:

1) Identification of the crack initiation area and propagation pattern, including beach marks and shear lips, at the macroscopic level.
2) Characterization of the microstructure around the fracture, including grain size and indications of plastic deformation or cleavage, to corroborate the failure mechanism.
3) High-resolution images from the crack initiation area to the propagation zone to confirm evidence of fatigue and surface features, such as dimples, using SEM.

4) Mechanical property data, including tensile strength, hardness, and ductility/elongation, obtained from destructive testing to compare the material performance with the HP pump design specifications provided in the existing design manual.

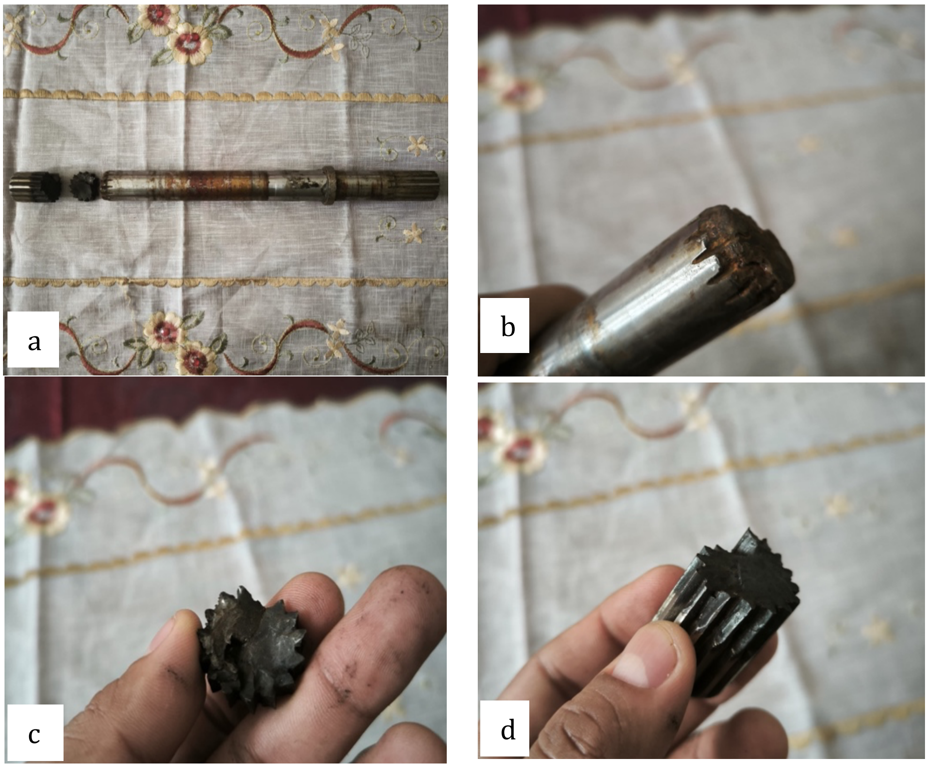

Figure 6. Failure Specimens: (a) HP Pump SWRO Test Specimen Experiencing Failure (b) Shaft as the Largest Part of the Fragment (c) Second Fragment on the Middle Side (d) Third Fragment as the End of the Shaft Coupled to the Pump Side

Planning techniques in the material testing process provided an overview and facilitated the effective and efficient execution of the tests. This included selecting the appropriate test methods, determining the relevant test parameters, and anticipating potential problems that might arise during the testing process.

In this study, the tests were conducted using a comparative method involving failed specimens and reference specimens obtained from non-failed areas, as shown in Figure 6. This comparative method was applied throughout the testing process. Careful test planning facilitated the collection of accurate and reliable data for the failure analysis.

The data processing stage involved transforming the collected data into complete information that could be used to address the research problems.

RESULTS AND DISCUSSION

Results

Chemical Composition

In the chemical composition test that was conducted, the Optical Emission Spectroscopy (OES) technique was used to determine the elemental composition of the materials. OES identifies elements by analyzing the characteristic wavelengths of light emitted by atoms in the test material after excitation (Li et al., 2026; Lough et al., 2020).

Table 1

Test Piece Chemical Composition Value Vs AISI 440A

Element (%)	A (%)	B (%)	AISI 440A ASTM A 276 (%)
C	0.54	0.63	0.6-0.75
Mn	0.86	0.34	1
P	0.02	0.02	0.04

Element (%)	A (%)	B (%)	AISI 440A ASTM A 276 (%)
S	0.01	0	0.03
Si	0.33	0.56	1
Cr	16.58	15.87	16-18
Mo	0.78	0.67	0.75
Fe	79.87	81.06	-

Based on the table above, the chemical compositions of Materials A and B are generally similar to that of AISI 440A. The carbon content of Material A is slightly below the specified range for AISI 440A (0.54%), whereas Material B has a chromium content below the specified range (15.87%).

Macrography

Macrography is a method used to examine the fracture surface and overall fracture characteristics of a metal specimen using the naked eye or low-magnification optical equipment. The method is intended to identify fracture patterns, including visible deformation, beach marks, chevron marks, and other features such as porosity on the fracture surface (Herdiana & Abidin, 2023; Manurung et al., 2020).

Figure 7. Macrostructure of Material A

Figure 8. Macrostructure of Material B

As shown in Figures 7 and 8, the fracture patterns in both materials exhibit predominantly brittle characteristics, with little or no visible plastic deformation around the failure areas. The pinion shaft gear sections appear relatively flat, and no necking is observed. In addition, rough line patterns are visible on the cross-sections of both materials. When these patterns are traced backward, they lead toward the respective crack-initiation areas.

Micrography

In contrast to macrography, micrography is a method used to examine the microstructure of a material using optical microscopy to determine features such as grain morphology, grain size, phase distribution, and crack-propagation paths (Li et al., 2026; Lough et al., 2020).

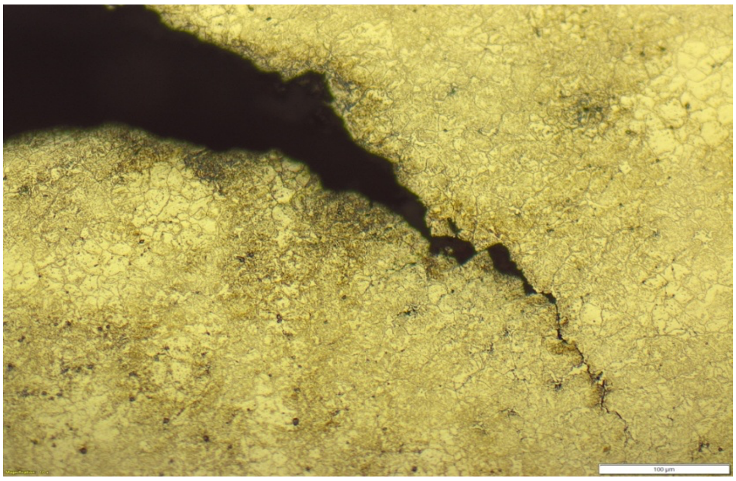

Figure 9. Imaging of Material Microstructure A

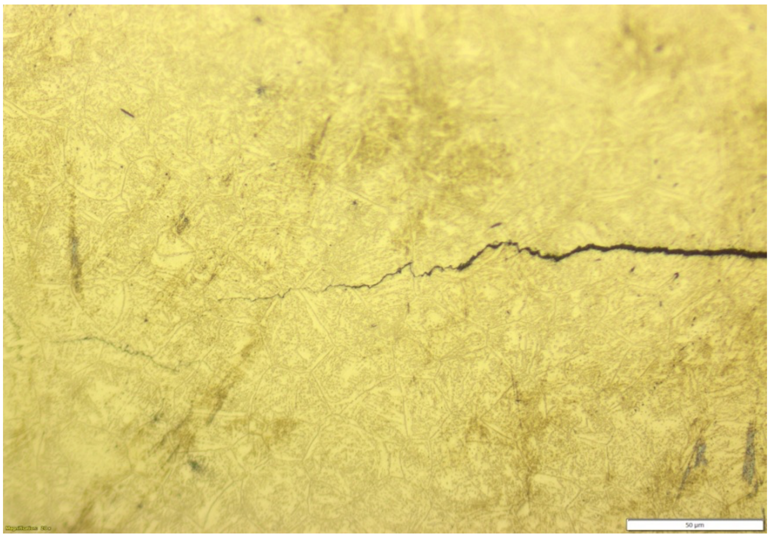

Figure 10. Microstructure Image of Material B

In Material A (Figure 9), the crack-propagation path is clearly visible through the grains, indicating a transgranular fracture mode. In contrast, Material B (Figure 10) exhibits microcrack propagation that predominantly follows the grain boundaries, indicating an intergranular fracture mode.

SEM

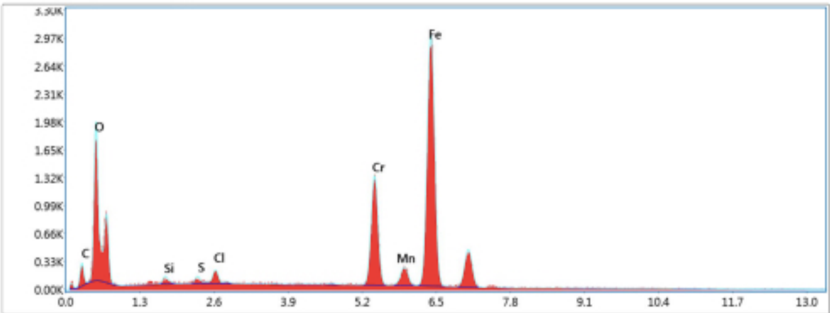

Smart Quant Results

Element	Weight %	Atomic %	Net Int.	Error %	Kratio	Z	A	F
C K	6.40	18.41	19.07	12.55	0.0179	1.2410	0.2252	1.0000
O K	14.21	30.70	141.25	7.99	0.0676	1.1934	0.3985	1.0000
SiK	0.58	0.71	8.86	15.72	0.0030	1.0952	0.4760	1.0033
S K	0.50	0.54	8.77	21.62	0.0038	1.0750	0.7065	1.0087
ClK	1.02	1.00	17.58	14.43	0.0084	1.0237	0.7884	1.0135
CrK	16.95	11.27	183.38	2.88	0.1716	0.9370	0.9968	1.0838
MnK	1.00	0.63	9.25	22.51	0.0097	0.9181	0.9979	1.0577
FeK	59.34	36.73	453.07	2.22	0.5382	0.9335	0.9690	1.0027

Figure 11. Content Spectrum in Material Fracture Area A

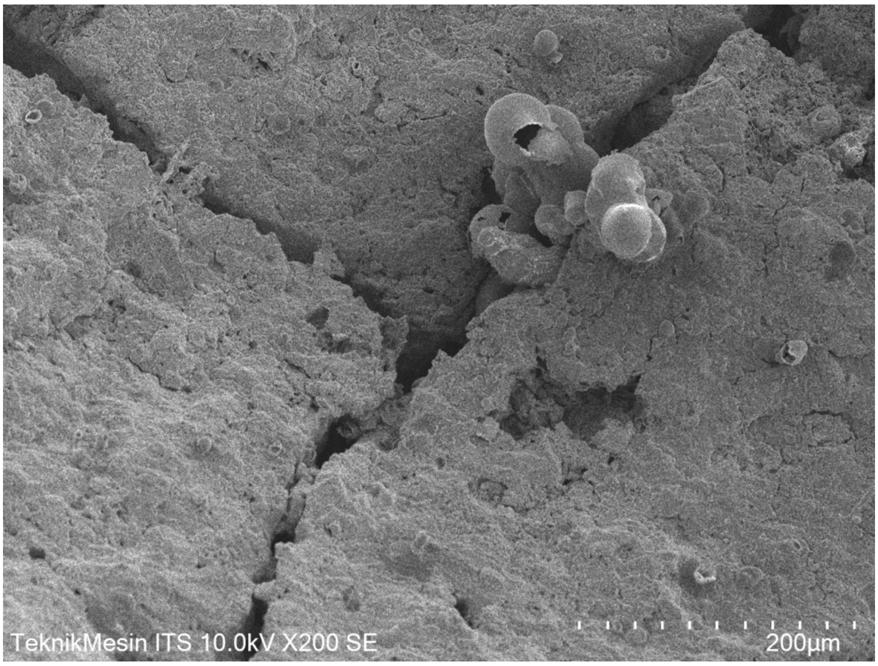

Figure 12. Appearance of Chromium Carbide Precipitate in Material A

In Material A, chromium carbide precipitates are observed, as shown in Figures 11 and 12. In Material B, chromium carbide precipitates are also indicated by the EDS results obtained from the fracture area (Figure 13). Meanwhile, the SEM image of Material B (Figure 14) clearly shows characteristics of brittle fracture, accompanied by microvoids and localized porosity on the fracture surface.

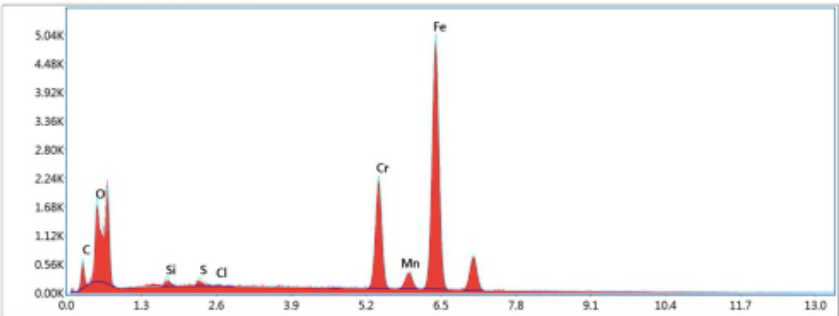

Smart Quant Results

Element	Weight %	Atomic %	Net Int.	Error %	Kratio	Z	A	F
C K	8.76	26.95	40.71	11.18	0.0250	1.2564	0.2273	1.0000
O K	6.60	15.24	93.89	8.91	0.0295	1.2084	0.3694	1.0000
SiK	0.78	1.02	18.10	13.02	0.0040	1.1094	0.4666	1.0032
S K	0.65	0.75	17.42	17.64	0.0050	1.0891	0.6961	1.0086
ClK	0.17	0.18	4.42	47.72	0.0014	1.0372	0.7784	1.0137
CrK	18.48	13.13	308.51	2.61	0.1893	0.9500	0.9958	1.0829
MnK	0.79	0.53	11.27	21.99	0.0078	0.9308	0.9966	1.0570
FeK	63.76	42.19	749.25	2.14	0.5837	0.9466	0.9650	1.0021

Figure 13. Content Spectrum in Fault Area B Material

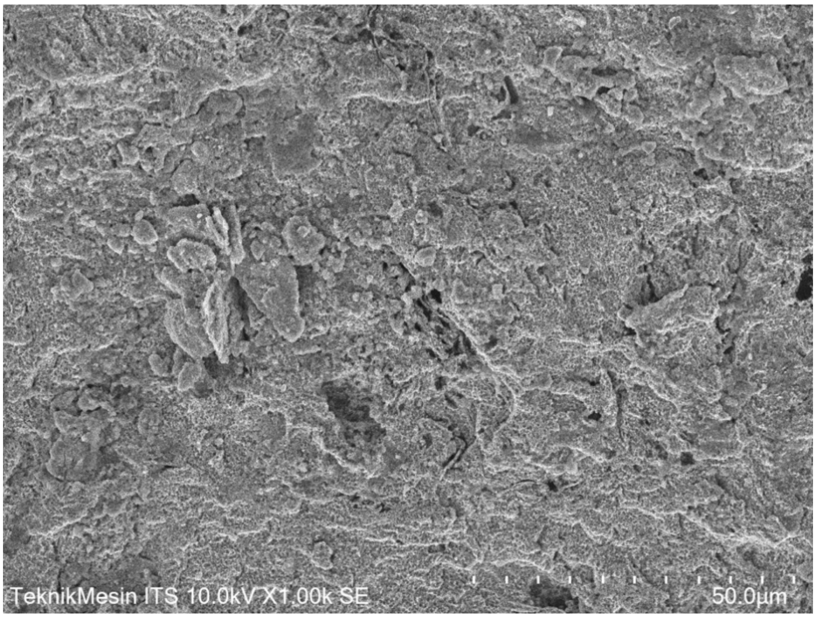

Figure 14. The Appearance of Micro-voids in Material B

Hardness Test

The hardness test is a method used to measure the resistance of a metal material to localized plastic deformation under an applied load and to provide an indication of its mechanical properties. In this study, hardness testing was performed using the Vickers method (Vickers hardness test) by collecting measurements from two specimen areas, namely the Reference Area and the Failure Area. The Reference Area was a portion of the specimen that was free from visible defects and was used as a reference and comparison with the Failure Area. The specimen had a thickness of 18 mm. The Failure Area was the portion of the specimen that had experienced failure (fracture) and represented the condition of the material in the failed region. Each area was tested at nine measurement points to determine the distribution of hardness values throughout the material.

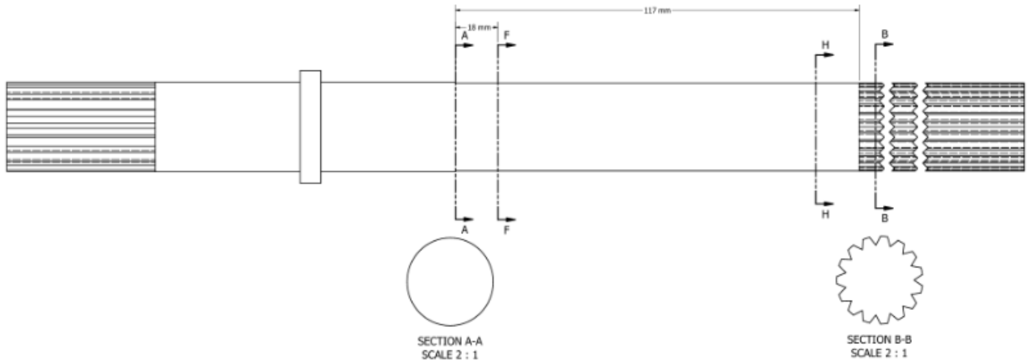

Figure 15. Material Hardness Test Specimen Processing Scheme A

Table 2

Hardness Test Value Area Reference Material A

Dot	Hardness (HV)	Image
1	377	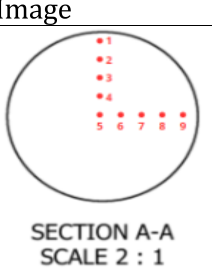
2	369	
3	347	
4	351	
5	386	
6	420	
7	407	
8	418	
9	414	
Average	387,66	

Table 3

Hardness Test Value Material Failure Area A

Dot	Hardness (HV)	Image
1	299	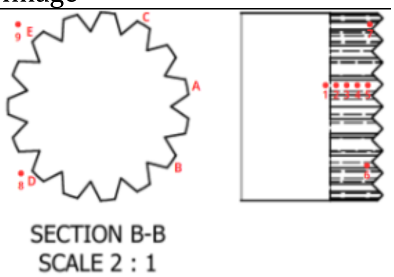
2	294	
3	314	
4	279	
5	306	
6	316	
7	300	
8	308	
9	333	
Average	305,44	

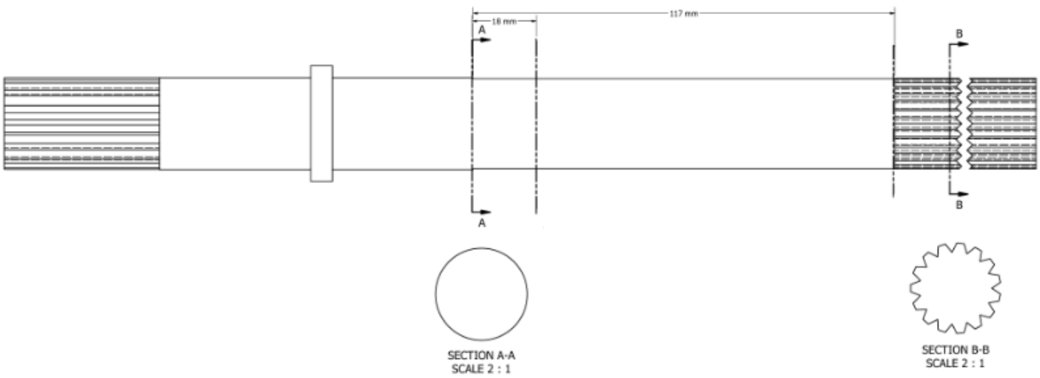

Figure 16. Material Hardness Test Specimen Processing Scheme B

Table 4

Hardness Test Value Area Reference Material B

Dot	Hardness (HV)	Image
1	340	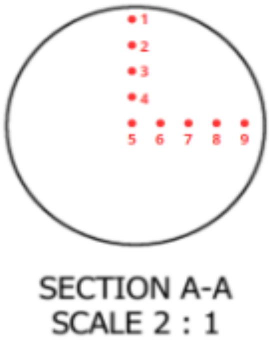
2	333	
3	329	
4	299	
5	327	
6	300	
7	304	
8	308	
9	316	
Average	317,33	

Table 5

Hardness Test Value Material Failure Area B

Dot	Hardness (HV)	Image
1	315	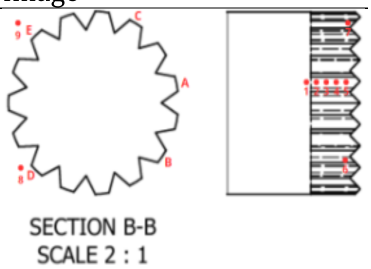
2	314	
3	303	
4	291	
5	279	
6	424	
7	314	
8	288	
9	288	
Average	312,89	

AISI 440A in the hardened condition can achieve a hardness of approximately 58 HRC, which corresponds to approximately 653 HV based on the ASTM E140 hardness-conversion table. The test results showed that the maximum hardness value obtained was only 424 HV (Table 6). The measurements also indicate variations in hardness across the specimen. In particular, the hardness values in some regions toward the center of the specimen tend to decrease, whereas the values measured closer to the upper surface, such as at Points 8 and 9, tend to be higher than the average value.

Discussion

Chemical Composition Analysis

The carbon content of Material A is lower than the specified range for AISI 440A (0.54% vs. 0.60–0.75%), which can contribute to reductions in the strength and hardness of the material (Kwak et al., 2022). In Material B, the chromium content is below the specified minimum value (15.87% vs. 16–18%). This deviation may reduce corrosion resistance because chromium is essential for the formation and maintenance of the protective chromium-oxide passive film on stainless steel (Łukaszczyk et al., 2021; Ma et al., 2026).

AISI 440A is a martensitic stainless steel known for its high strength and hardness and its resistance to wear and corrosion when appropriately heat treated. It is commonly used for components subjected to high mechanical and rotational loads, including bearings and other wear-resistant components (Kultamaa, 2022; Ovri et al., 2010). Given these characteristics, AISI 440A is potentially suitable as a shaft material for high-pressure SWRO pumps, provided that its composition and heat-treatment condition meet the required specifications. Therefore, deviations from the standard chemical composition, particularly the lower carbon content in Material A and the lower chromium content in Material B, may have contributed to the failure mechanism observed in the HP SWRO pump shaft.

Macrographic Analysis and Fracture Mechanism

The brittle fracture characteristics observed in both materials, including the absence of significant plastic deformation, relatively flat fracture surfaces, and the absence of necking, indicate that the final fracture occurred with limited macroscopic plastic deformation. These characteristics are consistent with the behavior of hardened martensitic stainless steel, which generally exhibits high hardness and strength but can have reduced toughness depending on its heat-treatment condition. The rough line patterns observed on the cross-sections and their apparent convergence toward the crack-initiation areas suggest that the fractures originated at localized stress-concentration sites and subsequently propagated through the material. The observed fracture features are consistent with a fatigue-failure mechanism that progressed toward a final rapid fracture after the crack had reached a critical size.

Micrographic Analysis and Crack-Propagation Patterns

The differences in crack-propagation patterns between the two materials provide important information regarding their respective fracture mechanisms. In Material A, the transgranular propagation pattern indicates that the crack propagated through the crystal grains. This fracture mode can occur under cyclic loading conditions, particularly when the grain boundaries provide greater resistance to crack propagation than the grain interiors. Consequently, the crack may preferentially propagate through the grains.

In contrast, the intergranular fracture pattern observed in Material B indicates that the grain boundaries acted as preferential paths for crack propagation. This phenomenon can occur because of impurity segregation at grain boundaries, excessive carbide precipitation along the grain boundaries, or corrosion-related degradation that reduces grain-boundary cohesion. In martensitic stainless steels, excessive or continuous carbide precipitation can also deplete chromium from the surrounding matrix, potentially reducing local corrosion resistance and promoting intergranular corrosion or sensitization. These differences in fracture mechanisms are important because each mechanism requires a different preventive and corrective approach.

SEM Analysis, Precipitation, and Heat-Treatment Effects

Carbide precipitation can occur during heat treatment and subsequent cooling processes and can significantly influence the mechanical and corrosion properties of stainless steel. The presence of chromium carbide precipitates in both materials indicates that carbide precipitation occurred during processing. The size, morphology, and distribution of these precipitates strongly influence the mechanical properties of the material. Finely dispersed and appropriately distributed precipitates can contribute to strengthening, whereas excessive coarsening or nonuniform distribution can reduce the effectiveness of precipitation strengthening (Lee et al., 2023). Excessive chromium carbide precipitation along grain boundaries can also reduce the chromium concentration in the adjacent matrix, thereby decreasing localized corrosion resistance and potentially promoting sensitization and intergranular corrosion.

In Material B, the presence of microvoids or localized porosity identified in the SEM images may have acted as stress-concentration sites and contributed to crack initiation. These microstructural discontinuities can accelerate crack nucleation and propagation, particularly under cyclic loading conditions associated with the operation of high-pressure SWRO pumps.

Hardness Analysis and Its Implications for Failure

The hardness of metallic materials is influenced by several factors, including chemical composition, heat-treatment conditions, and microstructural characteristics. Heat-treatment processes such as hardening and tempering can significantly affect hardness and other mechanical properties (Murmu et al., 2022; Srivastava et al., 2021). In addition, an increase in grain size can adversely affect certain mechanical properties, particularly yield strength, in accordance with the Hall–Petch relationship (Yahya, 2024). Hardness is closely related to several mechanical characteristics of the material, including strength, resistance to plastic deformation, wear resistance, and, depending on the microstructure, fatigue performance.

There is a substantial difference between the reference hardness associated with hardened AISI 440A (approximately 653 HV, corresponding to 58 HRC) and the measured hardness values of the two materials, with the maximum measured value being only 424 HV. This difference indicates that the materials did not attain the hardness level expected for AISI 440A in the referenced hardened condition. The relatively low hardness may be associated with an inadequate or nonuniform heat-treatment process and may reduce the material's resistance to wear and cyclic deformation, thereby increasing its susceptibility to fatigue damage under cyclic loading in the high-pressure SWRO pump shaft.

The nonuniform hardness distribution, characterized by lower hardness in some regions toward the center of the specimen and higher hardness near the upper surface, suggests variations in the heat-treatment response across the material. The central region may not have experienced sufficiently rapid or uniform cooling during quenching, resulting in incomplete martensitic transformation and the formation of a mixed microstructure with lower hardness. Such microstructural nonuniformity can create mechanically weaker regions that may act as preferential sites for crack initiation and subsequent fatigue-crack propagation.

Overall, the failure of the high-pressure SWRO pump shaft in both materials appears to have resulted from a combination of factors, including deviations in chemical composition from the AISI 440A specification, nonuniform carbide precipitation, hardness values substantially below those expected for the referenced hardened condition, and fracture characteristics indicative of limited plastic deformation and inadequate fracture toughness under the operating conditions. The combined effects of cyclic loading, stress concentrations, microstructural discontinuities, and nonuniform heat treatment may have promoted fatigue-crack initiation and subsequent propagation until final fracture.

CONCLUSION

Based on the results of the study, the failure of the HP SWRO pump shaft was associated with several factors, including nonuniform hardness in Materials A and B and hardness values substantially below those expected for AISI 440A in the referenced hardened condition. These conditions can adversely affect the strength, wear resistance, and fatigue performance of the material. In addition, indications of crack initiation were observed in the central regions of both test materials, with the lowest hardness value of 279 HV recorded at Point 4 in Material A and Point 5 in Material B. These findings were further supported by the micrographic observations. Material failure was also associated with the formation of chromium carbide precipitates, as identified through SEM and EDS analyses. The presence and nonuniform distribution of these precipitates may have altered the local mechanical and corrosion properties of the material and, particularly when concentrated along grain boundaries, may have contributed to embrittlement and intergranular crack propagation. Overall, the failure mechanism appears to have been influenced by an inappropriate or nonuniform heat-treatment process, which resulted in variations in carbide precipitation and hardness distribution throughout the material. These microstructural and mechanical-property variations may have created preferential sites for crack initiation and propagation, ultimately resulting in failure of the HP SWRO pump shaft.

ACKNOWLEDGEMENT

The authors express their sincere appreciation to Institut Teknologi Sepuluh Nopember for its academic support and to the personnel of UBP Labuhan Angin for the operational data and technical information that supported this research. The authors also thank all parties who provided valuable assistance during the material testing, data analysis, and preparation of this article.

AUTHOR CONTRIBUTION STATEMENT

Wandi Pagar Asi Napitupulu and Fahmi Mubarok jointly contributed to the conceptualization, research design, collection of operational and experimental data, material testing, failure analysis, interpretation of the findings, and preparation of the manuscript. Both authors participated in revising the article, approved the final version for publication, and agreed to be accountable for the accuracy and integrity of the work.

REFERENCES

Amin, M. K., Sulardjaka, & Saptadi, S. (2023). Performance Analysis And Techno Economy Of Post Overhaul Circulating Fluidized Bed Boiler Pltu. *International Journal Of Engineering And Computer Science*, *6*(1), 12–18. https://doi.org/10.21744/Ijecs.V6n1.2171

Dwiyoga, M. A. (2024). *Pengaruh Kenaikan Tegangan Dc Dan Konsentrasi Baking Soda 1, 2 Dan 3 Wt% Terhadap Elektron Transport Fasa H2o Pada Air Demineralisasi Dan Air Kondensasi* [Universitas Sultan Ageng Tirtayasa]. https://eprints.Untirta.Ac.Id/44329/

Herdiana, A., & Abidin, Z. (2023). Rancang Bangun Mesin Poles Untuk Proses Metalografi. *Seminar Teknologi Majalengka (STIMA)*, *7*, 92–100.

Inyang, U. E., & Olughu, C. O. (2025). The Importance Of Boiler Feed Water And Its Treatment In A Chemical Plant. *World Journal Of Advanced Research And Reviews*, *27*(1), 1624–1632. https://doi.org/10.30574/Wjarr.2025.27.1.2705

Joniarta, I. W., Dika, A. A., & Wijana, M. (2024). Analisis Efisiensi Pompa Sentrifugal Pada Desalinasi Dengan Proses Reverse Osmosis: Analysis Of Centrifugal Pump Efficiency In Desalination With The Reverse Osmosis Process. *Energy, Materials And Product Design*, *3*(2), 213–223. https://doi.org/10.29303/Empd.V3i2.5429

Kultamaa, M. (2022). *Functional Stainless Steel Porous Structures By Metal Injection Molding (Mim)*. Itä-Suomen Yliopisto.

Kwak, K., Mine, Y., Morito, S., Ohmura, T., & Takashima, K. (2022). Correlation Between Strength And Hardness For Substructures Of Lath Martensite In Low- And Medium-Carbon Steels. *Materials Science And Engineering: A*, *856*, 144007. https://doi.org/10.1016/J.Msea.2022.144007

Lee, G. H., Park, M., Kim, B., Jeon, J. B., Noh, S., & Kim, B. J. (2023). Evaluation Of Precipitation Phase And Mechanical Properties According To Aging Heat Treatment Temperature Of Inconel 718. *Journal Of Materials Research And Technology*, *27*, 4157–4168. https://doi.org/10.1016/J.Jmrt.2023.10.196

Li, Z., Zhang, Z., Chen, Y., Wang, Y., Du, Z., Zhang, Q., Huang, K., Su, Y., Wen, G., & Chen, X. (2026). In-Situ Optical Emission Spectroscopy Monitoring Of Laser Powder Bed Fusion Based On Spectral Data Prior Knowledge And Feature-Decision Level Fusion Network. *Mechanical Systems And Signal Processing*, *254*, 114406.

Lough, C. S., Escano, L. I., Qu, M., Smith, C. C., Landers, R. G., Bristow, D. A., Chen, L., & Kinzel, E. C. (2020). In-Situ Optical Emission Spectroscopy Of Selective Laser Melting. *Journal Of Manufacturing Processes*, *53*, 336–341. https://doi.org/10.1016/J.Jmapro.2020.02.016

Łukaszczyk, A., Banaś, J., Pisarek, M., Seyeux, A., Marcus, P., & Światowska, J. (2021). Effect Of Cr Content On Corrosion Resistance Of Low-Cr Alloy Steels Studied By Surface And Electrochemical Techniques. *Electrochem*, *2*(4), 546–562. https://doi.org/10.3390/Electrochem2040035

Ma, Q.-L., Zhu, X.-D., Zhao, P.-Y., Hong, R., Li, B., Liu, Q.-Y., Shang, C.-J., & Jia, S.-J. (2026). Fundamental Understanding Of Microstructure And Cr On Supercritical Co2 Corrosion Resistance Of High-Strength Low-Alloy Steels. *Journal Of Iron And Steel Research International*, *33*(4), 105.

Manurung, V. A. T., Wibowo, Y. T. J., & Baskoro, S. Y. (2020). *Panduan Metalografi*. Lp2m Politeknik Manufaktur Astra. Https://Repository.Polytechnic.Astra.Ac.Id/Files/Original/0fc5fc6144704d42442012e7e169fdf5573da7cb.Pdf

Murmu, S., Chaudhary, S. K., & Rajak, A. K. (2022). Effect Of Heat Treatment On Mechanical Properties Of Medium Carbon Steel Welds. *Materials Today: Proceedings*, *56*, 964–970.

Ovri, H., Ohaukwu, C. J., Bahadirov, K., Larsen, M., & Kjeldsteen, P. (2010). As-Sintered Aisi 440c Stainless Steels With Improved Hardness And Corrosion Resistance. *International Journal Of Powder Metallurgy*, *46*(6), 43–50. https://Publications.Hereon.De/Id/32570/

Rifai, A., Hartaja, D. R. K., Sulaeman, O., Setiadi, I., Ikhsan, I. N., Darmawangsa, M. R., Ardiana, C., Sofian, A., & Yunus. (2024). Pengaruh Tekanan Pada Reverse Osmosis Terhadap Penyisihan Kadar Ion Klorida (Cl-) Dan Total Dissolved Solids (TDS) Pada Pengolahan Air Payau. *Jurnal Teknologi Lingkungan*, *25*(2), 300–307. https://doi.org/10.55981/Jtl.2024.705

Srivastava, K., Sinha, A. A., & Sahani, R. (2021). Effect Of Heat Treatment On Hardness And

Toughness Of En8 Steel. *Materials Today: Proceedings*, *42*(Part 2), 1297–1303. https://doi.org/10.1016/J.Matpr.2020.12.1015

Wahyudin, A. R., Raihan, A., Adrian, M. F., Agustian, R., Darian, M. A., Ramadhan A, M. F., Paundra, F., & Ito, Y. (2024). Analisis Dan Perawatan Pada Water Treatment Plant (Wtp) Pltu X. *Perwira Journal Of Science & Engineering*, *4*(2), 86–93. https://doi.org/10.54199/Pjse.V4i2.306

Wulandari, F. A., & Alifah, A. S. A. N. (2026). Optimalisasi Transisi Energi Melalui Pembangkit Listrik Tenaga Nuklir Untuk Mewujudkan Clean Energy Di Indonesia. In *Proceeding Legal Symposium* (Vol. 4, Issue 1). https://doi.org/10.18196/Pls.V4i1.211

Yahya, H. M. (2024). Analisis Multiple Repair Dan Holding Time Post Weld Heat Treatment Material Sa 335 Grade P91 Dengan Proses Pengelasan Smaw Terhadap Nilai Kekerasan Dan Metalografi. In *Conference On Welding Engineering And Its Application (Cwea)* (Vol. 1, Issue 1, Pp. 7–14). Https://Journal.Ppns.Ac.Id/Index.Php/Cwea